How to cite: *Angew. Chem. Int. Ed.* **2023,** *62,* e202217100
International Edition: doi.org/10.1002/anie.202217100
German Edition: doi.org/10.1002/ange.202217100

Luminescence

Significant Enhancement of the Upconversion Emission in Highly Er^{3+}-Doped Nanoparticles at Cryogenic Temperatures

Langping Tu, Kefan Wu, Yongshi Luo, Enhui Wang, Jun Yuan, Jing Zuo, Ding Zhou, Bin Li, Jiajia Zhou, Dayong Jin,* and Hong Zhang**

Abstract: Relatively low efficiency is the bottleneck for the application of lanthanide-doped upconversion nanoparticles (UCNPs). The high-level doping strategy realized in recent years has not improved the efficiency as much as expected. It is argued that cross relaxation (CR) is not detrimental to upconversion. Here we combine theoretical simulation and spectroscopy to elucidate the role of CR in upconversion process of Er^{3+} highly doped (HD) UCNPs. It is found that if CR is purposively suppressed, upconversion efficiency can be significantly improved. Specifically, we demonstrate experimentally that inhibition of CR by introducing cryogenic environment (40 K) enhances upconversion emission by more than two orders of magnitude. This work not only elucidates the nature of CR and its non-negligible adverse effects, but also provides a new perspective for improving upconversion efficiency. The result can be directly applied to cryogenic imaging and wide range temperature sensing.

Introduction

Lanthanide (Ln^{3+}) doped upconversion nanomaterials can convert low energy photons to high energy emissions.[1] With their unique non-blinking and non-photobleaching anti-Stokes emissions,[2] upconversion nanomaterials have attracted numerous attention towards emerging applications, including volumetric displays,[3] multimodality bio-imaging,[4] photodynamic therapy,[5] high-security level anti-counterfeiting,[6] optogenetics,[7] and super-resolution imaging,[8] etc. Further developments require in-depth and comprehensive studies of the sophisticated upconversion process, as well as the rational design and controlled synthesis of nanomaterials toward high luminescence efficiencies. Albeit many targeted strategies, including organic dye sensitization,[9] plasmonic field modulation and enhancement,[10] surface phonon engineering in a thermal field,[11] and design of heterogeneous nanostructures,[12] have been exploited, and the reported upconversion efficiencies in the range of 0.03–10 % are already orders of magnitude higher than that of the conventional two-photon process of fluorophores.[13] To date, boosting upconversion brightness is still an urgent task.

Recent advances indicate that constructing highly doped upconversion nanoparticles (HD UCNPs) offers an emerging opportunity to enhance upconversion luminescence. With ultra-high densities of optical centers (i.e., active Ln^{3+}), HD UCNPs are expected to have greater light absorption and stronger energy transfer/migration process due to the accelerated ion-to-ion interactions. Nevertheless, the concomitant concentration quenching effect becomes inevitable,[14] which prevents HD UCNPs from achieving higher efficiency operations. Strategies, including high excitation irradiance,[15] dye sensitization,[16] inert shell passivation,[17] and heterogeneous nanostructure design,[18] have been developed to alleviate the deteriorating effect of concentration quenching, where impressive upconversion enhancement by the range of 10–1000 folds has been achieved.[14b]

[*] Dr. L. Tu, Prof. Y. Luo, Prof. D. Zhou, Prof. B. Li
State Key Laboratory of Luminescence and Applications, Changchun Institute of Optics, Fine Mechanics and Physics, Chinese Academy of Sciences
Changchun, Jilin, 130033 (China)
K. Wu, J. Yuan, Prof. H. Zhang
Van't Hoff Institute for Molecular Sciences, University of Amsterdam
Science Park 904, Amsterdam, 1098XH (The Netherlands)
E-mail: h.zhang@uva.nl
E. Wang, Dr. J. Zuo
Key Laboratory of Automobile Materials (Ministry of Education), College of Materials Science and Engineering, Jilin University
Changchun, 130025 (China)
Prof. J. Zhou, Prof. D. Jin
Institute for Biomedical Materials and Devices (IBMD), Faculty of Science, University of Technology Sydney
Sydney, NSW (Australia)
E-mail: jiajia.zhou@uts.edu.au
dayong.jin@uts.edu.au
Prof. D. Jin
UTS-SUSTech Joint Research Centre for Biomedical Materials and Devices, Department of Biomedical Engineering, College of Engineering, Southern University of Science and Technology
Shenzhen, Guangdong 518055 (China)

Despite remarkable progress being made in HD UCNPs, the physical insight into the sophisticated upconversion process within the nanosystem remain unclear. Numerical theoretical modeling is needed to quantify the advantages of the highly doped system, including the enhanced absorption and the accelerated ion-to-ion interactions. Especially considering that the gap between the theoretical simulations and experimental observations remains. For example, inert shell has been widely used to cut off the activators from the surface quenching sites and to eliminate the concentration quenching effect on erbium ions (Er^{3+}), so that the Er^{3+} doping concentrations have been increased from the conventional 2 mol % to 80–100 mol %,[17a,c] but the actual brightness fails to reach the expected level of enhancement, since the amount of activators has been increased by more than 40 folds ($NaYF_4$: 20 %Yb, 2 %Er@$NaYF_4$ versus $NaErF_4$:20 %Yb @$NaYF_4$ or $NaErF_4$@$NaYF_4$).[17c,19] Such a discrepancy suggests an ambiguous recognition of a luminescence mechanism playing a major role in the practical performance of such types of HD UCNPs.

Here, a Monte Carlo simulation suggests plenty of room for further promoting the upconversion brightness of Er^{3+}-rich core–shell structures (represented by the $NaErF_4$@$NaYF_4$). Experimentally, the expected upconversion enhancement by over two orders of magnitude was indeed observed in the cryogenic environment (e.g., cool down to 40 K). Different from the traditional view, our finding reveals that severe concentration quenching still exists in the inert shell passivated Er^{3+}-rich systems at room temperature. Spectral-domain and time-domain spectroscopic results indicate that the quenching is caused by the cascade Er^{3+}-Er^{3+} cross relaxation (CR), whose effectiveness strongly depends on the temperature. Furthermore, the trend was also observed in the Yb^{3+}/Er^{3+} "alloy" UCNPs (i.e., $NaYF_4$@$NaYb_{1-x}F_4$:Er_x@$NaYF_4$ core–shell-shell structures, where x varies from 2 % to 100 %). We found the optimal doping concentration of Er^{3+} activators towards the maximum brightness also varied with the temperature, e.g., 4 mol % at 250 K, 25 mol % at 150 K, 50 mol % at 75 K, and 100 mol % at 40 K. As a result, a significantly enhanced upconversion brightness by about 10 folds has been achieved, compared with the Er^{3+} low-doped alloy systems that have already been regarded as a kind of the most efficient upconversion nanostructures at room temperature. With a clearer insight into the temperature-responsive Er^{3+}-Er^{3+} CR effect, this work suggests a new scope for upconversion enhancement, low-temperature imaging, and wide-range temperature sensing.

Results and Discussion

In an ideal scenario, the macroscopic upconversion phenomena in Ln^{3+}-doped nanosystems can be rebuilt by a Monte Carlo simulation, in which upconversion luminescence is treated as a statistical result of numerous randomly walked excited states "collisions" (shown in Figure 1a and b). In our previous works,[20] a simulation model has been successfully set up for a traditional low doping upconversion system, i.e., $NaYF_4$: 20 %Yb, 2 %Er@$NaYF_4$. Our model quasi-quantitatively predicted the relevant upconversion efficiency since the ion-to-ion interaction parameters could be set appropriately from quantum mechanical calculations or experiments. However, experimental and simulated results diverge when directly applying this model to the upconversion systems with a high level of activators (e.g., $NaErF_4$@$NaYF_4$). According to the simulation, Er^{3+}-rich design is expected to largely promote the possibility of "collision" and thereby the upconversion efficiency because of the following advantages: 1) high level doping shortens the Ln^{3+}-to-Ln^{3+} average distance to 0.47 nm from 0.8 nm in traditional low doped UCNPs (LD UCNPs). Since the Ln^{3+}-to-Ln^{3+} interaction strength sharply decreases with the increase of ion-to-ion distance, the energy migration processes of the excited states will be accelerated by about two orders of magnitude.[1b] 2) In particular, $NaErF_4$@$NaYF_4$ has fully supplied "collision" sites for the migrated energy (Figure 1b), while in the traditional Y^{3+}/Yb^{3+}/Er^{3+} triplex-doping system only less than 10 % of grids participate in "collisions" (Figure 1a). Furthermore, via tuning the relevant parameters in the simulation model, the upconversion enhancement tiggered by these two advantages can be targeted investigated, which are evaluated to 71 and 7.7 folds, respectively (shown in Figure 1c). Relevant simulation details are discussed in the Supporting Information (Table S1, S2, Figure S1–S3). Combining these two positive factors, from 20 %Yb^{3+}, 2 %Er^{3+}

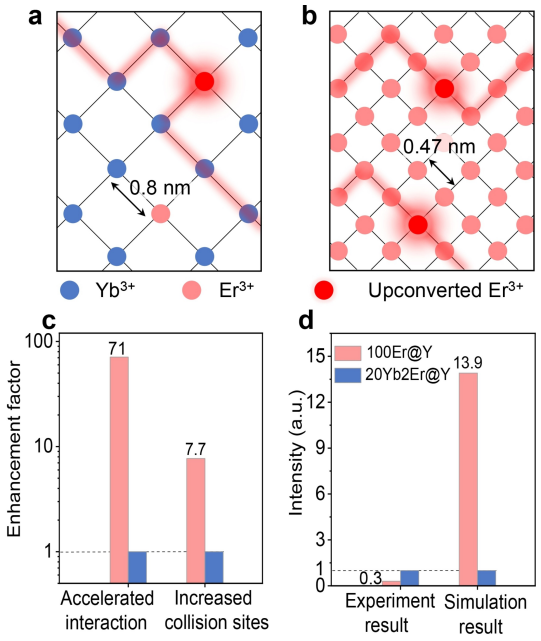

Figure 1. Schematic diagram of the randomly walked excited states "collision" triggering upconversion emission in a) a traditional $NaYF_4$: 20 %Yb, 2 %Er@$NaYF_4$ nanostructure, and b) a high level doped $NaErF_4$@$NaYF_4$ nanostructure. c) The simulated upconversion emission enhancement factors of $NaErF_4$@$NaYF_4$ nanostructure, induced by the accelerated ion-to-ion interaction and the increased "collision" sites, respectively. d) Comparison of experimental and simulated upconversion intensities of low doping (in blue) and high doping (in red) systems.

co-doping to 100 % Er^{3+} doping, an upconversion enhancement by 13.9 folds is expected from the simulation (Figure S4). Strikingly, the experimental result shows a huge discrepancy, in which the intensity of $NaErF_4$@$NaYF_4$ only reaches ≈30 % of that of $NaYF_4$: 20 %Yb, 2 %Er@$NaYF_4$ (Figure 1d).

Interestingly, the huge gap in luminescence brightness between the experimental and simulation results can be filled by introducing a cryogenic environment. To ensure fairness in comparison, controlled synthesis of pure hexagonal phase, uniform size, and structure (20 nm core with 5 nm thick shell) of UCNPs has been conducted. Their TEM images and XRD results are shown in Figure 2a and Figure S6. When the temperature decreases to 40 K, $NaErF_4$@$NaYF_4$ shows a sharply increased upconversion emission intensity by 170 folds upon the 0.1 W cm^{-2} 980 nm excitation, as shown in Figure 2b, c. While the intensity of the control sample of $NaYF_4$: 20 %Yb, 2 %Er@$NaYF_4$ varies little when the temperature decreases from 300 to 40 K, which is well in line with the previous reports.[21] For LD UCNPs (i.e., $NaYF_4$: 20 %Yb, 2 %Er@$NaYF_4$), the temperature-dependent intensity saturation appears at ≈160 K (2.2 folds stronger than the case at 300 K). Our observations resulted from the competition between the two opposite effects at the reduced temperature, i.e., the hindered Yb^{3+}→ Er^{3+} energy transfer (caused by retrogressive phonon activity) versus the restricted non-radiative energy loss. Note: due to the power-dependent intensity saturation, the cryogenic temperature induced enhancement factors also depend on the excitation power density, as it varies from 170 to 41 folds when increasing the excitation power density from 0.1 to 5 W cm^{-2} (Figure 2c and Figure S7). To provide more evidence for the cryogenic feeding effect, direct energy transfer between Er^{3+} ions without the participation of Yb^{3+} was also investigated with laser excitations at 800 nm (0.3 W cm^{-2}) and 1530 nm (0.03 W cm^{-2}), respectively. The results are shown in Figure 2d and Figure S8, S9, in which the same order of enhancement factors (97 folds and 98 folds, respectively) for $NaErF_4$@$NaYF_4$ have been achieved at 40 K. Furthermore, the results of the varying concentrations of singly-doped Er^{3+}, e.g., at 25 mol %, 50 mol %, and 75 mol %, are shown in Figure 2e and Figure S10. Subsequently, remarkable enhancement factors of 360 folds, 420 folds, and 260 folds have been achieved (under 0.1 W cm^{-2} 980 nm excitation).

The above results consistently indicate that besides the commonly recognized surface quenching, which is invalid in our case since a 5 nm-thick $NaYF_4$ inert shell is employed,[17a] a significant temperature-dependent concentration quenching of Er^{3+} exists in the relevant nanostructures. The cryogenic temperature in our case may sufficient to compensate the quenching effect when Er^{3+} is less than 50 mol %. However, when further increasing the concentration to 100 mol %, the compensation effect is reduced in view of the attenuated upconversion enhancing. In our opinion, the cryogenic environment proves to be effective for upconversion enhancement because Er^{3+}-to-Er^{3+} quenching interaction occurs through CR, whose

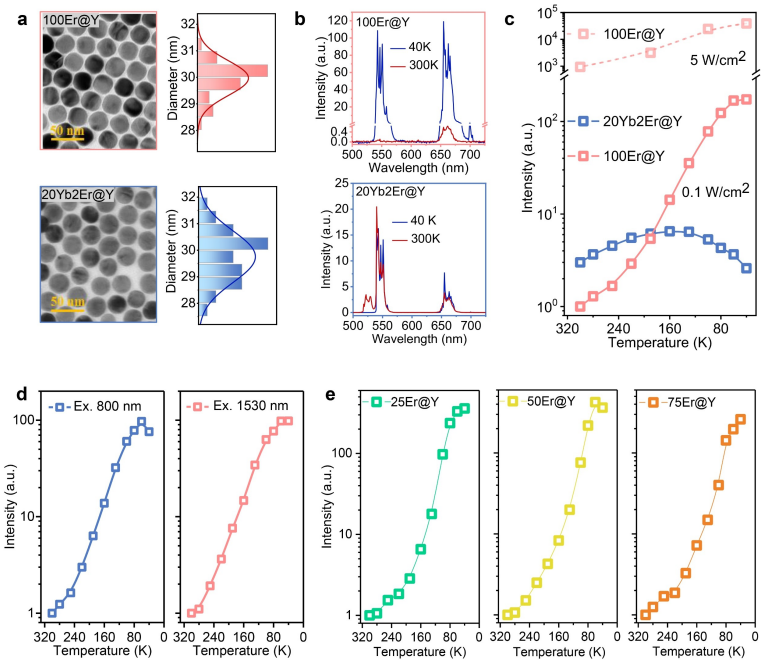

Figure 2. a) The TEM images of $NaErF_4$@$NaYF_4$ and $NaYF_4$: 20%Yb, 2%Er@$NaYF_4$ nanostructures and the statistical result of the particles' size distribution. b) Temperature dependent (40 and 300 K) upconversion emission spectra of the two nanostructures, respectively. c) The integral upconversion emission intensities (from 500 to 700 nm) of the two nanostructures at different temperatures. Laser excitations are at 980 nm with power densities of 0.1 W cm^{-2} and 5 W cm^{-2}, respectively. d) Temperature dependent upconversion emission intensities of $NaErF_4$@$NaYF_4$ under the laser excitations of 800 nm (0.3 W cm^{-2}) and 1530 nm (0.03 W cm^{-2}), respectively. e) Temperature dependent upconversion emission intensities of series $NaYF_4$: x%Er@$NaYF_4$ nanostructures (x = 25, 50, 75). Laser excitations are at 980 nm with power density of 0.1 W cm^{-2}.

probability is temperature dependent. It is worth noting that CR has long been recognized as one of the most active vital factors that quench the brightness in LD UCNPs,[22] and some inspiring works have investigated the Er^{3+}-Er^{3+} (or Er^{3+}-Yb^{3+}) CR-caused energy loss in the bare core,[23] or Er^{3+} relatively low-doped structures (e.g., 10 %).[24] So far, the CR role in the core–shell HD UCNPs is still debatable,[25] or even believed to be harmless.[17a] Here, we show CR becomes crucial in enhancing the brightness of the Er^{3+} highly doped upconversion system.

To date, most investigations for CR in HD UCNPs are focused on its role in the emission ratio modulation, for example, leading to a relatively high red/green (R/G) emission ratio in Er^{3+}-rich core–shell structures,[17,26] with the corresponding CR paths being illustrated in Figure 3a (upper part). However, here we find the degrees of upconversion emission quenching and the R/G emission ratio increasing, caused by CR, are highly correlated. As shown in Figure 3b, accompanied by the huge enhancement in luminescence intensity, the R/G emission ratio of HD UCNPs (i.e., $NaErF_4$@$NaYF_4$) dramatically drops from 30.2 to 1.46 when the temperature decreases from 300 to 40 K. This is because that for Er^{3+}-rich core–shell systems at the relatively high temperatures, the lattice vibration (i.e., phonons) facilitates to fill the energy gaps in various CR processes. When some particular CR paths enable the green→red emission transfer (Figure 3a upper part), the depletion of upconversion energy is also efficient via the cascade CR processes (i.e., green/red→NIR (near-infrared) or green→red→NIR transfer, as illustrated in Figure 3a lower part). By introducing a cryogenic environment, lattice vibration is restricted, and as a result, both the green→red emission transfer and the cascade energy degradation processes will be hindered, leading to a massive accumulation of excited states on the green/red emission energy levels. This experimental result is further supported by our Monte Carlo simulation results. As shown in Figure 3c, compared with the situation without CR, once a proper CR strength is included in HD UCNPs (i.e., $2.1\times10^5\ s^{-1}$, whose value is close to the calculated Er^{3+}-Er^{3+} energy migration strength in the HD UCNPs), a reasonable emission quenching (100-fold, with intensity decreases from 1 to 0.01) can indeed be obtained (modelling details are described in Figure S5), which also explains the observed discrepancy in Figure 1c. Notably, this evaluated CR strength (i.e., $2.1\times10^5\ s^{-1}$) also predicts a fast decay lifetime ($\approx$5 μs) for the corresponding energy level of Er^{3+} (i.e., $^4S_{3/2}$), which is indeed qualitatively observed in our measurements (Figure 3e right and Table S3).

Next, to further determine the influence of CR, we investigated the temperature-dependent PL dynamics when exciting Er^{3+} at 488 nm with nanosecond pulses. As shown in Figure 3e (left), the down-shifting 540 nm emission decay curves of LD UCNPs ($NaYF_4$:20 %Yb,2 %Er@$NaYF_4$ as control) at the $^4S_{3/2}$ energy level exhibit a mild temperature dependence (time decay curves in the range of 0–2500 μs are shown in Figure S11). The decay time decreases from 430 to 166 μs with temperatures increasing from 40 to 300 K. This mild variation mainly reflects the temperature-dependent non-radiative relaxation since CR plays a relatively weak role in LD UCNPs. In contrast, the down-shifting 540 nm emission decay curves of HD UCNPs (i.e., $NaErF_4$@$NaYF_4$) display a large variation in response to the temperature changes (Figure 3e right, Figure S11 and Table S3), which exhibits a typical multi-exponential decay at the relatively high temperatures. As illustrated in Figure 3d, the depopulation processes of the $^4S_{3/2}$ energy level of HD UCNPs contain both the radiative/non-radiative relaxations (insensi-

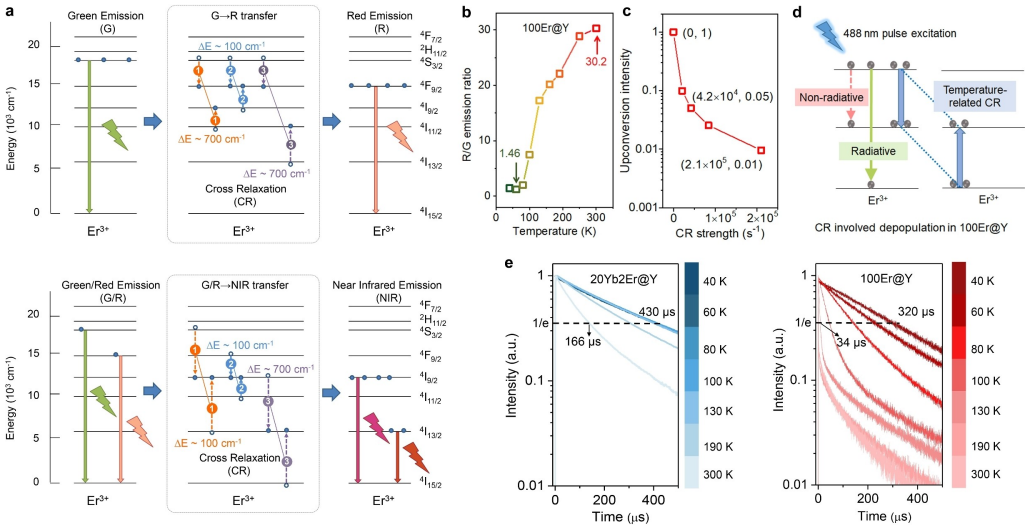

Figure 3. a) Several typical Er^{3+}-Er^{3+} CR processes are involved in the green→red emission shift (upper part), and green/red→NIR emission shift (lower part). The same color arrows in groups represent the electron transitions in the same CR process. b) The temperature dependent green/red upconversion emission ratio of $NaErF_4$@$NaYF_4$ nanostructure. Laser excitation is at 980 nm with a power density of 0.1 $W\,cm^{-2}$. c) The simulated relationship between Er^{3+}-Er^{3+} CR strength and upconversion emission intensity. d) The depopulation processes in $NaErF_4$@$NaYF_4$, including radiative/non-radiative relaxations and temperature-related CR processes. e) The temperature dependent 540 nm emission decay curves of low-doped $NaYF_4$:20%Yb,2%Er@$NaYF_4$ (left) and high-doped $NaErF_4$@$NaYF_4$ (right). Excitation: 488 nm pulsed laser.

tive to temperature) and CR (sensitive to temperature). Therefore, the slow decay component (decreasing from 320 to 118 μs as the temperature increases from 40 to 300 K) in Figure 3e (right) can be well attributed to the varied radiative and non-radiative relaxations from individual excited states. Then, the significantly accelerated decay of less than 34 μs reflects the Er^{3+}-Er^{3+} CR effect in HD UCNPs, which obviously dominates the depopulation process when the temperature is above 100 K (Figure 3e right and Figure S12). These results reconfirm that CR in Er^{3+}-rich systems plays a major role in quenching the emissions at relatively high temperatures, and employing cryogenic temperature can restrict CR and thereby enhance the brightness of HD UCNPs.

Once the role of CR in Er^{3+} singly doped HD UCNPs is understood, our conclusive finding can be further applied to investigate a series of Yb^{3+}/Er^{3+} "alloy" systems (i.e., $NaYF_4$@$NaYb_{1-x}Er_xF_4$@$NaYF_4$, x increases from 2 mol % to 100 mol %). According to the previous reports,[19,27] via fully utilizing the space of nanostructure (i.e., the sum of the concentrations of Yb^{3+} and Er^{3+} reaches 100 mol %), the "alloy" system has already been reported as one of the most efficient inorganic upconversion structures, therefore, further improving its efficiency is meaningful. The series of core–shell–shell structures are synthesized with uniform sizes and morphologies for spectroscopy comparison (Figure 4a and Figure S13, S14), where the size of the inert core and the thickness of the active shell and the inert shell are measured as 26 nm, 6 nm, and 6 nm, respectively. In line with our expectation, for the Er^{3+}-rich "alloy" systems (with the Er^{3+} concentration above 25 mol %), cryogenic temperature (e.g., 40 K) can significantly enhance the upconversion emission brightness by around two orders of magnitude (Figure 4b). The enhancement mechanism can also be attributed to the Er^{3+}-Er^{3+} CR suppression in the cryogenic environment. Thererfore, when reducing the temperature from 300 to 40 K, the optimized doping concentration of Er^{3+} in "alloy" system needs to be correspondingly increased from 4 mol % to 100 mol % to produce the brightest "alloy" UCNPs. Remarkably, compared with the brightest design at 300 K (Er^{3+} at 4 mol %, Figure S15), an around 10-fold upconversion enhancement has been achieved for the Er^{3+} heavily doped "alloy" UCNPs (over 50 mol %) in the cryogenic environment (Figure 4b).

Next, we take a closer look into the role of Yb^{3+} in tuning the R/G emission ratios of "alloy" structures. Notably, for the "alloy" systems heavily doped with both Yb^{3+} and Er^{3+} (i.e., $NaYF_4$@$NaYb_{1-x}Er_xF_4$@$NaYF_4$, $0.25 \leq x \leq 0.75$, labeled as dual HD alloy UCNPs), their R/G emission ratio becomes extremely high, even at the presence of the cryogenic environment, e.g., 95 folds at 40 K for $NaYF_4$@$NaYb_{0.5}Er_{0.5}F_4$@$NaYF_4$. In stark contrast, the robust green emissions were observed at 40 K when either Yb^{3+} or Er^{3+} is low-doped (i.e., R/G emission ratios are less than 5-fold if $x \leq 0.15$ or $x = 1.0$, shown in Figure 5a). Similar trends can be well observed within a relatively wide temperature range (i.e., 50–160 K, Figure S16). This suggests that for the dual HD alloy UCNPs in the cryogenic environment, 1) impressive red upconversion enhancement (from $^4F_{9/2}$ state) can still be observed due to the Er^{3+}-Er^{3+} CR suppression, and 2) on the contrary, for the green emission (from $^4S_{3/2}$ state), an efficient depopulation path is still in hiding, which cannot be simply attributed to the Er^{3+}-Er^{3+} CR. This opinion can be further confirmed by the down-shifting PL dynamics at 540 nm (under 488 nm pulsed excitation). As shown in Figure 5b, different from the control groups of $NaY_{0.5}Er_{0.5}F_4$@$NaYF_4$ and $NaYF_4$@$NaYb_{0.98}Er_{0.02}F_4$ @$NaYF_4$, a fast decay process of as quick as 11.2 μs, representing the existence of efficient depopulation, can only be observed from the dual HD alloy UCNPs (i.e., $NaYF_4$@$NaYb_{0.5}Er_{0.5}F_4$@$NaYF_4$).

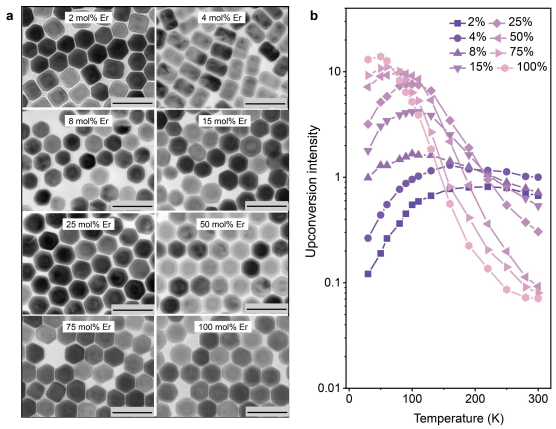

Figure 4. a) The TEM images of $NaYF_4$@$NaYb_{1-x}Er_xF_4$@$NaYF_4$ series of "alloy" UCNP systems, where x increases from 2 mol % to 100 mol %. Scale bars: 100 nm. b) The temperature-dependent upconversion emission intensities (integral from 500 to 700 nm) of the series of Yb/Er "alloy" systems. All the samples are excited by a 0.1 W cm^{-2} 980 nm laser.

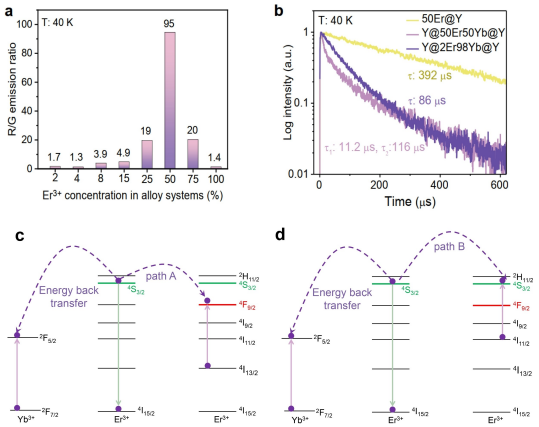

Figure 5. a) At 40 K, the R/G emission ratios of the series of alloy UCNPs when the Er^{3+} concentration increases from 2 mol % to 100 mol %. b) At 40 K, the luminescence decay curves of the $NaY_{0.5}Er_{0.5}F_4$@$NaYF_4$ (yellow line), $NaYF_4$@$NaYb_{0.5}Er_{0.5}F_4$@$NaYF_4$ (light purple line) and $NaYF_4$@$NaYb_{0.98}Er_{0.02}F_4$ @$NaYF_4$ (dark purple line) nanostructures. c), d) Schematic diagrams of the two paths of Er^{3+}-Er^{3+}-Yb^{3+} tri-ion interaction. All the samples are excited by a 0.1 W cm^{-2} 980 nm laser.

All the above observations cannot be explained by the simple interactions between any two types of ions, including Er^{3+}-Er^{3+} and Er^{3+}-Yb^{3+} interactions, otherwise high R/G emission ratios should be also observed in either Er^{3+} or Yb^{3+} singly HD alloy UCNPs in cryogenic environment (i.e., $x=1$ or 0.02). Therefore, we proposed a Yb^{3+}-Er^{3+}-Er^{3+} tri-ion interaction model that follows a $^2F_{7/2}(Yb^{3+})+{}^4S_{3/2}(Er^{3+})+{}^4I_{13/2}(Er^{3+})\rightarrow{}^2F_{5/2}(Yb^{3+})+{}^4I_{15/2}(Er^{3+})+{}^4F_{9/2}(Er^{3+})$ cooperative energy transfer process. As illustrated in Figure 5c, d, due to the simple energy level structure, the most possible role of Yb^{3+} in R/G emission modulation is to follow an Er^{3+} ($^4S_{3/2}$)→Yb^{3+} ($^2F_{7/2}$) energy back transfer process, where an upward transition on another excited Er^{3+} should be simultaneously involved (to cover the excess energy). Among the two possible transition paths, i.e., Path A of $^4I_{13/2}$ to $^4F_{9/2}$ and Path B of $^4I_{11/2}$ to $^4S_{3/2}$, since the lifetime of $^4I_{13/2}$ state is around 10 times longer than that of $^4I_{11/2}$ state, Path A dominates, leading to the high R/G emission ratio. Without the assistance of Yb^{3+} of a relatively larger absorption cross-section at 980 nm–1.2×10^{-20} cm^2,[28] it is unlikely for the $NaErF_4$@$NaYF_4$ system to achieve a high R/G ratio, as due to the relatively smaller absorption cross-section of Er^{3+} at 980 nm–1.7×10^{-21} cm^2.[28] The accordingly energy back transfer process, i.e., Er^{3+} ($^4S_{3/2}$)→Er^{3+} ($^4I_{15/2}$), will be much less effective than the Er^{3+} ($^4S_{3/2}$)→Yb^{3+} ($^2F_{7/2}$) process.

Conclusion

With both the theoretical modelling and spectroscopic characterization results, we confirm that for the Er^{3+}-rich HD UCNPs systems (either Er^{3+} singly doped or co-doped with Yb^{3+}), besides the well-recognized surface-related energy quenching processes, the cascade phonon-assisted Er^{3+}-Er^{3+} CR plays a dominant role in the upconversion energy loss at room temperature. A cryogenic environment can suppress the harmful CR, so that the upconversion brightness will be significantly enhanced by orders of magnitude. Furthermore, a large R/G upconversion emission ratio can be achieved in the Yb^{3+}/Er^{3+} dual HD "alloy" systems, where a cooperative energy transfer process, i.e., $^2F_{7/2}(Yb^{3+})+{}^4S_{3/2}(Er^{3+})+{}^4I_{13/2}(Er^{3+})\rightarrow{}^2F_{5/2}(Yb^{3+})+{}^4I_{15/2}(Er^{3+})+{}^4F_{9/2}(Er^{3+})$, has been first identified. Our findings record the upper limit of the upconversion brightness of Yb^{3+}/Er^{3+} "alloy" systems, and suggest the new strategies to develop more efficient HD UCNPs.

Acknowledgements

This work was financially supported by the Natural Science Foundation of China (12104179, 62075217, 11874355, 11874354, 61575194, 22172154, 62075215, 51720105015), Jilin Provincial Department of Science and Technology (Grants 20210101148JC, 202512JC010475440), the Shenzhen Science and Technology Program (KQTD20170810110913065; 20200925174735005), Fundamental Research Funds for the Central Universities, JLU., and the Dutch Research Council (NWO) in the framework of the Fund New Chemical Innovation under grant nr. 731.015.206, NWO TTW perspective project MEDPHOT, EU H2020-MSCA-ITN-ETN Action program, ISPIC, under grant nr. 675743, EU H2020MSCA-RISE-2017 Action program, CANCER, under grant nr. 777682.

Conflict of Interest

The authors declare no conflict of interest.

Data Availability Statement

The data that support the findings of this study are available from the corresponding author upon reasonable request.

Keywords: Cross Relaxation · High-Level Doping · Monte Carlo Simulations · Temperature · Upconversion Nanoparticle

[1] a) G. Chen, H. Qiu, P. N. Prasad, X. Chen, *Chem. Rev.* **2014**, *114*, 5161–5214; b) F. Auzel, *Chem. Rev.* **2004**, *104*, 139–173.
[2] S. Wu, G. Han, D. J. Milliron, S. Aloni, V. Altoe, D. V. Talapin, B. E. Cohen, P. J. Schuck, *Proc. Natl. Acad. Sci. USA* **2009**, *106*, 10917–10921.
[3] R. Deng, F. Qin, R. Chen, W. Huang, M. Hong, X. Liu, *Nat. Nanotechnol.* **2015**, *10*, 237–242.
[4] a) F. Wang, D. Banerjee, Y. Liu, X. Chen, X. Liu, *Analyst* **2010**, *135*, 1839–1854; b) J. Zhou, Z. Liu, F. Li, *Chem. Soc. Rev.* **2012**, *41*, 1323–1349.
[5] a) N. M. Idris, M. K. Gnanasammandhan, J. Zhang, P. C. Ho, R. Mahendran, Y. Zhang, *Nat. Med.* **2012**, *18*, 1580–1585; b) J. Xu, R. Shi, G. Chen, S. Dong, P. Yang, Z. Zhang, N. Niu, S. Gai, F. He, Y. Fu, J. Lin, *ACS Nano* **2020**, *14*, 9613–9625; c) J. Xu, P. Yang, M. Sun, H. Bi, B. Liu, D. Yang, S. Gai, F. He, J. Lin, *ACS Nano* **2017**, *11*, 4133–4144.
[6] X. Liu, Y. Wang, X. Li, Z. Yi, R. Deng, L. Liang, X. Xie, D. T. B. Loong, S. Song, D. Fan, A. H. All, H. Zhang, L. Huang, X. Liu, *Nat. Commun.* **2017**, *8*, 899.
[7] a) X. Liu, H. Chen, Y. Wang, Y. Si, H. Zhang, X. Li, Z. Zhang, B. Yan, S. Jiang, F. Wang, S. Weng, W. Xu, D. Zhao, J. Zhang, F. Zhang, *Nat. Commun.* **2021**, *12*, 5662; b) S. Chen, A. Z. Weitemier, X. Zeng, L. He, X. Wang, Y. Tao, A. J. Y. Huang, Y. Hashimotodani, M. Kano, H. Iwasaki, L. P. Parajuli, S. Okabe, D. B. L. Teh, A. H. All, I. Tsutsui-Kimura, K. F. Tanaka, X. Liu, T. J. Mchugh, *Science* **2018**, *359*, 679–683.
[8] a) Y. Liu, Y. Lu, X. Yang, X. Zheng, S. Wen, F. Wang, X. Vidal, J. Zhao, D. Liu, Z. Zhou, C. Ma, J. Zhou, J. A. Piper, P. Xi, D. Jin, *Nature* **2017**, *543*, 229–233; b) Q. Zhan, H. Liu, B. Wang, Q. Wu, R. Pu, C. Zhou, B. Huang, X. Peng, H. Agren, S. He, *Nat. Commun.* **2017**, *8*, 1058; c) S. Wen, Y. Liu, F. Wang, G. Lin, J. Zhou, B. Shi, Y. D. Suh, D. Jin, *Nat. Commun.* **2020**, *11*, 6047.
[9] W. Zou, C. Visser, J. A. Maduro, M. S. Pshenichnikov, J. C. Hummelen, *Nat. Photonics* **2012**, *6*, 560–564.
[10] a) W. Park, D. Lu, S. Ahn, *Chem. Soc. Rev.* **2015**, *44*, 2940–2962; b) J. He, W. Zheng, F. Ligmajer, C. Chan, Z. Bao, K. Wong, X. Chen, J. Hao, J. Dai, S. Yu, D. Y. Lei, *Light: Sci. Appl.* **2017**, *6*, e16217.
[11] J. Zhou, S. Wen, J. Liao, C. Clarke, S. A. Tawfik, W. Ren, C. Mi, F. Wang, D. Jin, *Nat. Photonics* **2018**, *12*, 154–158.

[12] a) M. Haase, H. Schaefer, *Angew. Chem. Int. Ed.* **2011**, *50*, 5808–5829; *Angew. Chem.* **2011**, *123*, 5928–5950; b) Y. F. Wang, G. Y. Liu, L. D. Sun, J. W. Xiao, J. C. Zhou, C. H. Yan, *ACS Nano* **2013**, *7*, 7200–7206; c) H. S. Qian, Y. Zhang, *Langmuir* **2008**, *24*, 12123–12125; d) F. Vetrone, R. Naccache, V. Mahalingam, C. G. Morgan, J. A. Capobianco, *Adv. Funct. Mater.* **2009**, *19*, 2924–2929.

[13] a) J. C. Boyer, F. C. J. M. van Veggel, *Nanoscale* **2010**, *2*, 1417–1419; b) S. Fischer, N. D. Bronstein, J. K. Swabeck, E. M. Chan, A. P. Alivisatos, *Nano Lett.* **2016**, *16*, 7241–7247.

[14] a) S. Wen, J. Zhou, K. Zheng, A. Bednarkiewicz, X. Liu, D. Jin, *Nat. Commun.* **2018**, *9*, 2415; b) B. Chen, F. Wang, *Acc. Chem. Res.* **2020**, *53*, 358–367.

[15] a) J. Zhao, D. Jin, E. P. Schartner, Y. Lu, Y. Liu, A. V. Zvyagin, L. Zhang, J. M. Dawes, P. Xi, J. A. Piper, E. M. Goldys, T. M. Monro, *Nat. Nanotechnol.* **2013**, *8*, 729–734; b) D. J. Gargas, E. M. Chan, A. D. Ostrowski, S. Aloni, M. V. P. Altoe, E. S. Barnard, B. Sanii, J. J. Urban, D. J. Milliron, B. E. Cohen, P. J. Schuck, *Nat. Nanotechnol.* **2014**, *9*, 300–305.

[16] W. Wei, G. Chen, A. Baev, G. S. He, W. Shao, J. Damasco, P. N. Prasad, *J. Am. Chem. Soc.* **2016**, *138*, 15130–15133.

[17] a) N. J. J. Johnson, S. He, S. Diao, E. M. Chan, H. Dai, A. Almutairi, *J. Am. Chem. Soc.* **2017**, *139*, 3275–3282; b) Q. Chen, X. Xie, B. Huang, L. Liang, S. Han, Z. Yi, Y. Wang, Y. Li, D. Fan, L. Huang, X. Liu, *Angew. Chem. Int. Ed.* **2017**, *56*, 7605–7609; *Angew. Chem.* **2017**, *129*, 7713–7717; c) J. Zuo, Q. Li, B. Xue, C. Li, Y. Chang, Y. Zhang, X. Liu, L. Tu, H. Zhang, X. Kong, *Nanoscale* **2017**, *9*, 7941–7946; d) C. Ma, X. Xu, F. Wang, Z. Zhou, D. Liu, J. Zhao, M. Guan, C. I. Lang, D. Jin, *Nano Lett.* **2017**, *17*, 2858–2864.

[18] a) X. Chen, L. Jin, W. Kong, T. Sun, W. Zhang, X. Liu, J. Fan, S. F. Yu, F. Wang, *Nat. Commun.* **2016**, *7*, 10304; b) J. Wang, R. Deng, M. A. MacDonald, B. Chen, J. Yuan, F. Wang, D. Chi, T. S. A. Hor, P. Zhang, G. Liu, Y. Han, X. Liu, *Nat. Mater.* **2014**, *13*, 157–162.

[19] B. Tian, A. Fernandez-Bravo, H. Najafiaghdam, N. A. Torquato, M. V. P. Altoe, A. Teitelboim, C. A. Tajon, Y. Tian, N. J. Borys, E. S. Barnard, M. Anwar, E. M. Chan, P. J. Schuck, B. E. Cohen, *Nat. Commun.* **2018**, *9*, 3082.

[20] a) J. Zuo, D. Sun, L. Tu, Y. Wu, Y. Cao, B. Xue, Y. Zhang, Y. Chang, X. Liu, X. Kong, W. J. Buma, E. J. Meijer, H. Zhang, *Angew. Chem. Int. Ed.* **2018**, *57*, 3054–3058; *Angew. Chem.* **2018**, *130*, 3108–3112; b) Y. Feng, Z. Li, Q. Li, J. Yuan, L. Tu, L. Ning, H. Zhang, *Light: Sci. Appl.* **2021**, *10*, 105.

[21] K. Wu, J. Cui, X. Kong, Y. Wang, *J. Appl. Phys.* **2011**, *110*, 053510.

[22] a) J. F. Suyver, J. Grimm, M. K. van Veen, D. Biner, K. W. Krämer, H. U. Güdel, *J. Lumin.* **2006**, *117*, 1–12; b) F. Vetrone, J. C. Boyer, J. A. Capobianco, A. Speghini, M. Bettinelli, *Chem. Mater.* **2003**, *15*, 2737–2743.

[23] L. Li, N. Zhao, L. Fu, J. Zhou, X. Ai, J. Zhang, *Nano Res.* **2018**, *11*, 2104–2115.

[24] B. Zhou, B. Tang, C. Zhang, C. Qin, Z. Gu, Y. Ma, T. Zhai, J. Yao, *Nat. Commun.* **2020**, *11*, 1174.

[25] T. Sun, Y. Li, W. L. Ho, Q. Zhu, X. Chen, L. Jin, H. Zhu, B. Huang, J. Lin, B. E. Little, S. T. Chu, F. Wang, *Nat. Commun.* **2019**, *10*, 1811.

[26] a) R. Joshi, R. S. Perala, S. B. Shelar, A. Ballal, B. P. Singh, R. S. Ningthoujam, *ACS Appl. Mater. Interfaces* **2021**, *13*, 3481–3490; b) J. Zuo, L. Tu, Q. Li, Y. Feng, I. Que, Y. Zhang, X. Liu, B. Xue, L. J. Cruz, Y. Chang, H. Zhang, X. Kong, *ACS Nano* **2018**, *12*, 3217–3225.

[27] Q. Liu, Y. Zhang, C. S. Peng, T. Yang, L. M. Joubert, S. Chu, *Nat. Photonics* **2018**, *12*, 548–553.

[28] L. Tu, X. Liu, F. Wu, H. Zhang, *Chem. Soc. Rev.* **2015**, *44*, 1331–1345.

Manuscript received: November 21, 2022
Accepted manuscript online: December 13, 2022
Version of record online: January 10, 2023